Band structure of nickel: Spin-orbit coupling, the Fermi surface, and the optical conductivity*

C. S. Wang and J. Callaway
Department of Physics and Astronomy, Louisiana State University, Baton Rouge, Louisiana 70803
(Received 7 December 1973)

A previous self-consistent calculation of energy bands in ferromagnetic nickel using the tight-binding method has been extended to include spin-orbit coupling. Exchange was incorporated using the $X\alpha$ method with $\alpha = 2/3$. Energy levels were obtained at 1357 points in 1/16th of the Brillouin zone. The direction of spin alignment was taken to be [001]. The density of states was computed by a hybrid method. Cross sections of the Fermi surface were determined, and effective masses were obtained. The interband contribution to the conductivity tensor was calculated using matrix elements computed from wave functions including spin-orbit coupling. Results were obtained for both the diagonal and the off-diagonal elements of the conductivity tensor.

I. INTRODUCTION

This paper reports an extension of a previous band calculation for ferromagnetic nickel to include the effects of spin-orbit coupling.[1] Results are presented for the density of states, the Fermi surface, and the optical conductivity tensor. A detailed comparison of theory and experiment is attempted.

Spin-orbit coupling is of major significance in a description of the properties of ferromagnetic transition metals. It leads to the existence of magnetic anisotropy, the anomalous Hall effect, and magneto-optical effects. Substantial modifications of the Fermi surface result from changes in the connectivity of the energy bands. Attempts have been made to study spin-orbit effects in the band structure of nickel for more than 30 years.[2-10] Much of this work, however, has been based on oversimplified tight-binding models of the d band structure. Other investigations have employed interpolation schemes designed to fit empirical information concerning the band structure, magnetic properties, and Fermi surfaces.[7,10] We are not aware of previous attempts to include spin-orbit coupling into a first-principles band calculation for this metal.

The plan of this paper is as follows. We summarize, in the remainder of this introduction, the essential features of the calculation reported in Ref. 1 on which this work is based. Section II contains a discussion of the methods employed to incorporate the spin-orbit interaction and an outline of the procedures of the present calculation. The method used to calculate the density of states is described in Sec. III. Our results for Fermi-surface properties are presented in Sec. IV and are compared with experiment. The calculation of the optical conductivity is summarized in Sec. V. Finally, our general conclusions are stated in Sec. VI.

The band calculation described in Ref. 1 employed the tight-binding method as reformulated by Lafon and Lin.[11] The following set of basis functions was used: Atomic wave functions for all states except $3d$ (e.g., $1s$, $2s$, $3s$, $4s$, $2p$, $3p$, and and $4p$) were represented by the linear combination of Gaussian-type orbitals (GTO) determined by Wachters[12] from a self-consistent field calculation for the free nickel atom. Five independent GTO were introduced for each of the five $l=2$ angular functions. The orbital exponents used in defining these functions were the same as employed by Wachters. Exchange was included according to the $X\alpha$ approximation[13] with $\alpha=\frac{2}{3}$.[14] The Hamiltonian and overlap matrices are of dimension 38×38. Since a spin-polarized potential was employed, separate matrix problems result for states of majority and minority spins. The potential for the first iteration of the self-consistent calculation was obtained from the superposition of neutral atom (d^9s^1) charge densities. The techniques employed in the iterations to achieve self-consistency have been described elsewhere.[15] Eleven iterations were required to achieve self-consistency. In the final three iterations, the charge density was sampled at 89 points in $\frac{1}{48}$th of this Brillouin zone. The calculated energies were found to be in reasonably good agreement with those obtained in a self-consistent augmented-plane-wave (APW) calculation by Connolly.[16] We will not repeat a detailed description of the results.

II. SPIN-ORBIT COUPLING

The calculation previously described was extended by the inclusion of spin-orbit coupling.

Other relativistic effects were neglected. Introduction of spin-orbit coupling into a band calculation for a ferromagnet causes substantial complications. First, since spin-orbit coupling connects states of ↑ and ↓ spin, the size of the Hamiltonian matrix is increased (in our case 76×76), and the elements become complex. This causes a considerable increase in computing time. Second, the symmetry group is reduced. The appropriate group theory has been presented by Falicov and Ruvalds.[17] In addition, the band structure depends on the direction of spin alignment. Separate band structures must be computed for each direction spin alignment investigated. However, because of limitations of computer time, we have restricted our calculations to a single direction of spin alignment: the [001] axis.

The computation of the matrix elements of the spin-orbit interaction was performed as follows. The additional term in the Hamiltonian has the form

$$H_{so} = \frac{\hbar}{4m^2c^2}\vec{\sigma}\cdot(\nabla V \times \vec{p}) . \tag{2.1}$$

The potential V used in Eq. (2.1) was that obtained in Ref. 1 from the self-consistent band calculation, expressed as a Fourier series

$$V = \sum_s V(\vec{K}_s) e^{i\vec{K}_s\cdot\vec{r}} . \tag{2.2}$$

The same Gaussian-orbital basis set was used for this calculation as in Ref. 1. Use of Gaussian orbitals is advantageous, as all matrix elements of the H_{so} can be reduced to sums of simple analytic functions of the reciprocal-lattice vectors. We found in several tests that the only nonnegligible matrix elements of H_{so} are those in the p-p and d-d blocks, with orbitals centered on the same atomic site ("central cell").

Since this calculation appears to be the first for nickel in which the spin-orbit coupling strength is not simply regarded as an adjustable parameter, we will give some details below. The central-cell matrix elements of H_{so} have the following form:

$$H_{so} = \begin{pmatrix} v_1 & v_2 \\ -v_2^* & v_1^* \end{pmatrix} \tag{2.3}$$

in which the spin states considered are ↑, ↓, respectively. The forms of the submatrices v_1 and v_2 are as follows for the p-p block:

$$\langle p\uparrow|v_1|p\uparrow\rangle = \begin{pmatrix} 0 & iA & 0 \\ -iA & 0 & 0 \\ 0 & 0 & 0 \end{pmatrix} . \tag{2.4}$$

The spatial symmetries of the basis states are (in order) x, y, z:

$$\langle p\uparrow|v_2|p\downarrow\rangle = \begin{pmatrix} 0 & 0 & -A \\ 0 & 0 & iA \\ A & -iA & 0 \end{pmatrix} . \tag{2.5}$$

In these equations,

$$A = (3/4\pi)N\sum_{\vec{K}} V(\vec{K})\vec{K}^2 F(\vec{K}) , \tag{2.6}$$

in which

$$F(\vec{K}) = \frac{\hbar^2}{24m^2c^2}\pi^{3/2}u^{5/2}e^{-u\vec{K}^2/4} \tag{2.7}$$

and

$$u = \frac{1}{\alpha_1+\alpha_2} . \tag{2.8}$$

The sums include all reciprocal-lattice vectors; α_1 and α_2 are the exponents of the Gaussian orbitals; thus

$$\phi_{p_x}(\alpha_1, r) = [2(2\alpha_1)^{5/2}/\pi^{3/2}]^{1/2} x e^{-\alpha_1 r^2} , \tag{2.9}$$

and N is the product of the appropriate normalization constants. The corresponding formulas for the d-d block are,[18] with states arranged in the order xy, yz, xz, x^2-y^2, $3z^2-r^2$,

$$\langle d\uparrow|v_1|d\uparrow\rangle = \begin{bmatrix} 0 & 0 & 0 & iB & 0 \\ 0 & 0 & iC & 0 & 0 \\ 0 & -iC & 0 & 0 & 0 \\ -iB & 0 & 0 & 0 & 0 \\ 0 & 0 & 0 & 0 & 0 \end{bmatrix} , \tag{2.10}$$

$$\langle d\uparrow|v_2|d\downarrow\rangle = \begin{bmatrix} 0 & C & -iC & 0 & 0 \\ -C & 0 & 0 & -\frac{iB}{2} & -\frac{i\sqrt{3}}{2}B \\ iC & 0 & 0 & -\frac{B}{2} & \frac{\sqrt{3}}{2}B \\ 0 & \frac{iB}{2} & \frac{B}{2} & 0 & 0 \\ 0 & \frac{i\sqrt{3}}{2}B & -\frac{\sqrt{3}}{2}B & 0 & 0 \end{bmatrix} , \tag{2.11}$$

where

$$B = \frac{15}{4\pi}\frac{Nu}{4}\sum_{\vec{K}} V(\vec{K})F(\vec{K}) \times[\alpha_2 u^2(K_x^4+K_y^4+K_z^4) + (2\alpha_1-\alpha_2)u^2(K_x^2K_y^2+K_y^2K_z^2+K_z^2K_x^2) - 4\vec{K}^2] , \tag{2.12}$$

$$C = \frac{15}{4\pi}\frac{Nu}{4}\sum_{k} V(K)F(K)[u(K_x^2K_y^2+K_y^2K_z^2 + K_z^2K_x^2) - 2\vec{K}^2] . \tag{2.13}$$

All of the basis functions are assumed to be normalized with respect to the angular integrations so that N depends on the orbital exponents only. Spherical symmetry of the potential has not been assumed in writing these formulas. There are, in this case, two independent constants involved in the d-d spin-orbit Hamiltonian. In fact, spherical symmetry is a good approximation, since it is the potential close to a nucleus which is important. For a spherically symmetric potential, we have simply

$$B = 2C = \xi ,$$

where ξ is the usual spin-orbit coupling parameter if atomic wave functions are employed in the usual form, $H_{so} = \xi \vec{L} \cdot \vec{S}$.

In our calculation, the spin-orbit parameters A, B, C, depend on the indices of the pair of orbital functions used in calculating the matrix elements. In order to compare calculations of properties of nickel which are dependent on spin-orbit coupling, it is useful to compute an equivalent atomic spin-orbit coupling parameter. This calculation was performed with the wave functions of Wachters[12] and our self-consistent potential. We found $\xi = 0.0067$ Ry. This result is somewhat larger than the atomic value $\xi = 0.0055$ Ry. The difference between B and $2C$ was found to be zero within the accuracy of our calculation.

The Hamiltonian including exchange and spin-orbit coupling was diagonalized at 1357 points in $\frac{1}{16}$th of the Brillouin zone. The lattice parameter was taken as 6.644 a.u. The calculated band structure is shown along certain symmetry lines in Fig. 1. Some calculated energy levels at symmetry points are listed in Table I. Since the actual symmetry group for this problem does not permit a particularly informative classification of states, we have labeled states at symmetry points in Fig. 1 in terms of the predominant component; that is, neglecting the mixing of states of majority and minority spin components. This labeling is possible since spin-orbit coupling is small compared to the exchange splitting.

It will be noticed that the band structure shown in Fig. 1 is quite similar to that formed by superposing the majority and minority spin bands obtained in Ref. 1. However, spin-orbit coupling removes many of the accidental degeneracies present in such a picture. The interplay of spin-orbit and exchange effects can be illustrated by considering the points X. In the present case, there are two inequivalent points of this type which are not connected by an operation of the symmetry group: these are denoted $X(0, 0, 1)$ and $X(1, 0, 0)$. Since the exchange splitting is large compared to spin-orbit coupling, we can qualitatively consider the latter as a perturbation. Specifically, let us consider the states $X_{5\downarrow}$ near the top of the d band. For $X(1, 0, 0)$, the basis functions are of the sym-

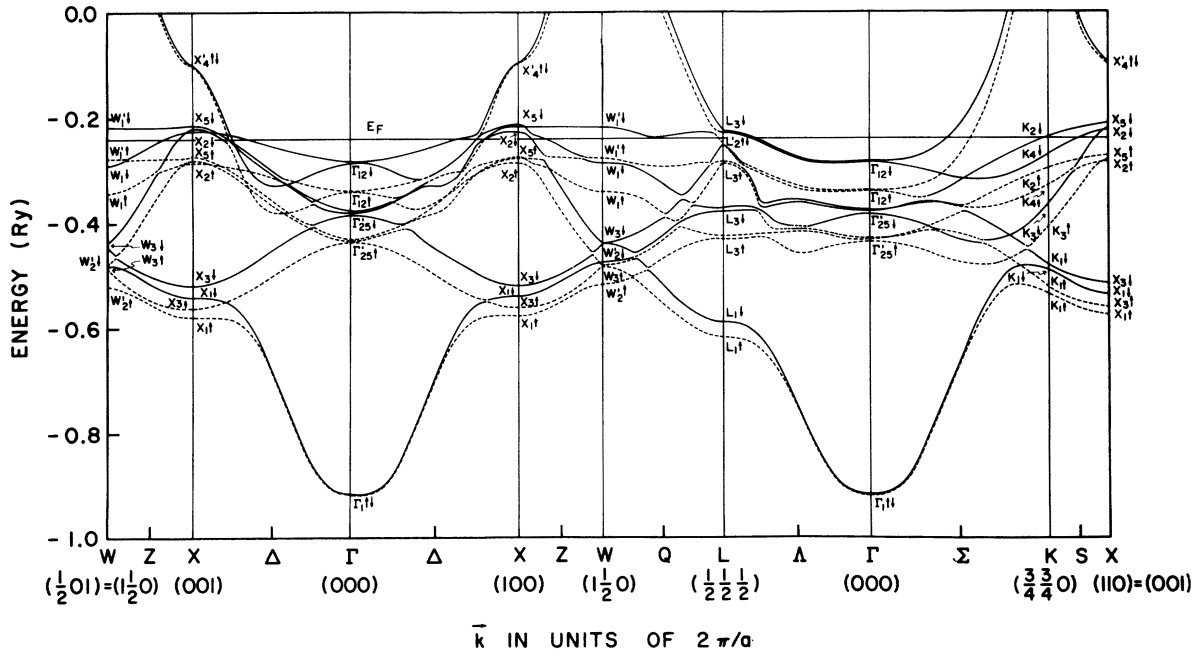

FIG. 1. Band structure of nickel along some symmetry lines in the Brillouin zone. States are labeled according to the symmetry of the largest spin component. The solid lines indicate states of minority spin, the dashed lines of majority spin.

TABLE I. Energy levels at symmetry points (Ry).

Band	Γ (0, 0, 0)	X (1, 0, 0)	X(0, 0, 1)	L ($\frac{1}{2}$, $\frac{1}{2}$, $\frac{1}{2}$)	W (1, $\frac{1}{2}$, 0)	W (1, 0, $\frac{1}{2}$)	K ($\frac{3}{4}$, $\frac{3}{4}$, 0)	K ($\frac{3}{4}$, 0, $\frac{3}{4}$)
12	−0.2850 (Γ_{12}^+)	−0.0983 ($X_4'^+$)	−0.0983 ($X_4'^+$)	−0.2264 (L_3^+)	0.2978 (W_3^+)	0.3057 (W_3^+)	0.1709 (K_3^+)	0.1709 (K_3^+)
11	−0.2851 (Γ_{12}^+)	−0.0993 ($X_4'^+$)	−0.0993 ($X_4'^+$)	−0.2300 (L_3^+)	0.2978 (W_3^+)	0.2937 (W_3^+)	0.1519 (K_3^+)	0.1519 (K_3^+)
10	−0.3408 (Γ_{12}^+)	−0.2149 (X_5^+)	−0.2124 (X_5^+)	−0.2520 ($L_2'^+$)	−0.2164 ($W_1'^+$)	−0.2164 ($W_1'^+$)	−0.2368 (K_2^+)	−0.2367 (K_2^+)
9	−0.3413 (Γ_{12}^+)	−0.2160 (X_5^+)	−0.2203 (X_5^+)	−0.2521 ($L_2'^+$)	−0.2766 ($W_1'^+$)	−0.2766 ($W_1'^+$)	−0.2703 (K_4^+)	−0.2707 (K_4^+)
8	−0.3778 ($\Gamma_{25}'^+$)	−0.2272 (X_2^+)	−0.2255 (X_2^+)	−0.2860 (L_3^+)	−0.2881 (W_1^+)	−0.2881 (W_1^+)	−0.2967 (K_2^+)	−0.2962 (K_2^+)
7	−0.3808 ($\Gamma_{25}'^+$)	−0.2758 (X_5^+)	−0.2736 (X_5^+)	−0.2898 (L_3^+)	−0.3429 (W_1^+)	−0.3428 (W_1^+)	−0.3272 (K_4^+)	−0.3273 (K_4^+)
6	−0.3854 ($\Gamma_{25}'^+$)	−0.2773 (X_5^+)	−0.2805 (X_5^+)	−0.3736 (L_3^+)	−0.4387 (W_3^+)	−0.4357 (W_3^+)	−0.3670 (K_3^+)	−0.3669 (K_3^+)
5	−0.4304 ($\Gamma_{25}'^+$)	−0.2869 (X_2^+)	−0.2859 (X_2^+)	−0.3803 (L_3^+)	−0.4389 (W_3^+)	−0.4428 (W_3^+)	−0.4090 (K_3^+)	−0.4091 (K_3^+)
4	−0.4338 ($\Gamma_{25}'^+$)	−0.5179 (X_3^+)	−0.5178 (X_3^+)	−0.4263 (L_3^+)	−0.4766 ($W_2'^+$)	−0.4736 ($W_2'^+$)	−0.4837 (K_1^+)	−0.4836 (K_1^+)
3	−0.4365 ($\Gamma_{25}'^+$)	−0.5398 (X_1^+)	−0.5398 (X_1^+)	−0.4330 (L_3^+)	−0.4815 (W_3^+)	−0.4823 (W_3^+)	−0.4929 (K_1^+)	−0.4929 (K_1^+)
2	−0.9144 (Γ_1^+)	−0.5619 (X_3^+)	−0.5619 (X_3^+)	−0.5873 (L_1^+)	−0.4833 (W_3^+)	−0.4848 (W_3^+)	−0.5219 (K_1^+)	−0.5219 (K_1^+)
1	−0.9155 (Γ_1^+)	−0.5775 (X_1^+)	−0.5774 (X_1^+)	−0.6178 (L_1^+)	−0.5183 ($W_2'^+$)	−0.5182 ($W_2'^+$)	−0.5359 (K_1^+)	−0.5359 (K_1^+)

metry $xy\downarrow$, $xz\downarrow$. Spin-orbit coupling does not connect these states; instead there is coupling between these and other majority and minority spin states. Since these states are separated from $X_{5\downarrow}$, the splitting of $X_{5\downarrow}$ is small (0.0012 Ry). On the other hand, for $X(0, 0, 1)$, the basis functions are $zy\downarrow, zx\downarrow$. There is a nonzero spin-orbit matrix element between these states, leading to the considerably larger splitting (0.0078 Ry).

III. DENSITY OF STATES

Gilat has reviewed different methods of calculating the density of states.[19] We employ here the Gilat-Raubenheimer[20] method in combination with an interpolation scheme. The method is similar to that used by Cooke and Wood,[21] except that our interpolation procedure is based on second-order $\vec{k}\cdot\vec{p}$ perturbation theory. The band calculation included 1357 points in $\frac{1}{16}$th of the Brillouin zone. Energies, wave functions, and momentum matrix elements were obtained at these points. A finer mesh was constructed by dividing the original step size by three—this represents 26 additional points around each previous general point. The $\vec{k}\cdot\vec{p}$ calculation was performed as follows. If a given band at the "original" point ($\vec{k}_0$) was separated by 0.005 Ry or more from all other bands, ordinary perturbation theory was employed to determine the energy at the additional points $\vec{k}$. Thus

$$E_n(\vec{k}) = E_n(\vec{k}_0) + \frac{\hbar}{m}(\vec{k}-\vec{k}_0)\cdot\vec{\pi}_{nn} + \frac{\hbar^2}{2m}(\vec{k}^2-\vec{k}_0^2) + \frac{\hbar^2}{m^2} \times \sum_{j(j\neq n)} \frac{[(\vec{k}-\vec{k}_0)\cdot\vec{\pi}_{nj}][(\vec{k}-\vec{k}_0)\cdot\vec{\pi}_{jn}]}{E_n(\vec{k}_0)-E_j(\vec{k}_0)} . \tag{3.1}$$

The matrix element is

$$\vec{\pi}_{nj} = \frac{(2\pi)^3}{\Omega}\int u_n^*(\vec{k}_0,\vec{r})[\vec{p}+(\hbar/4mc^2) \times\vec{\sigma}\times\nabla V(\vec{r})]u_j(\vec{k}_0,\vec{r})d^3r , \tag{3.2}$$

in which Ω is the volume of the cell and u is the cell periodic part of the Bloch function. Numerical tests showed that the spin-orbit contribution to the matrix element [the term in (3.2) proportional to $(\vec{\sigma}\times\nabla V)$] was negligible; hence in practice $\vec{\pi}_{nj}$ was always replaced by $\vec{p}_{nj}$. Only 12 bands were included in the sum in (3.1). Thus, the second-order term is not computed exactly, but since the other energy denominators are much larger, the accuracy should be sufficient. When two or more bands at $\vec{k}_0$ were separated by less than 0.005 Ry, an effective Hamiltonian was diagonalized. The elements of this Hamiltonian are

$$H_{ln}(k)=[E_l(\vec{k}_0)+\frac{\hbar^2}{2m}(\vec{k}-\vec{k}_0)^2]\delta_{ln}+\frac{\hbar}{m}(\vec{k}-\vec{k}_0)\cdot\vec{\pi}_{ln}$$
$$+\frac{\hbar^2}{m^2}\sum_j{}'\frac{[(\vec{k}-\vec{k}_0)\cdot\vec{\pi}_{lj}][(\vec{k}-\vec{k}_0)\cdot\vec{\pi}_{jn}]}{E_A-E_j(k_0)}\,, \tag{3.3}$$

in which E_A is the average energy of the nearly degenerate levels at $\vec{k}_0$. The prime on the sum indicates that the nearly degenerate levels are excluded. As before, only 12 bands were included in the sum in (3.3), so that second-order term is not exact.

The linear analytic integration scheme was then applied to each minicell constructed around each mesh point.[20] Projection operators were used to separate the contributions from majority and minority spins to the density of states. Our results for the majority- and minority-spin-state densities and for the total are shown in Figs. 2–4. The total density of states at the Fermi energy was found to be 23.56 electrons/atom Ry. The magneton number was found to be 0.62, somewhat higher than the experimental value of 0.56.[22] Our calculation predicts that a minority spin hole pocket associated with the $X_{2\downarrow}$ level should exist. This has not been observed experimentally, although it has also been predicted by other self-consistent calculations.[23] This hole pocket is probably responsible for the disagreement between theoretical and experimental values of the magneton number.

IV. FERMI SURFACE

The Fermi surface of nickel has been carefully studied through measurements of the de Haas-van Alpen effect[23–27] and cyclotron resonance.[28] These observations are of great importance in that they confirm the general picture of itinerant-electron ferromagnetism in nickel, in which the electrons responsible for magnetic order are not localized, but instead have wave functions extending throughout the crystal and contribute to the formation of a Fermi surface.

The major features of the Fermi surface of nickel can be understood on the basis of a calculation in which spin-orbit coupling is neglected, but this interaction must be included in a detailed comparison of theory and experiment.[29] As was noted above, the spin-orbit splitting of the states $X_{5\downarrow}(0, 0, 1)$ and $X_{5\downarrow}(1, 0, 0)$ is quite different. This leads to a significant difference in the sizes of the hole pockets around these points and to large anisotropy of de Haas–van Alpen frequencies.[25] A rapid variation of the de Haas–van Alpen amplitude when the applied magnetic field is tilted a few degrees from the [110] direction in a $(1\,\bar{1}\,0)$ plane has been interpreted as resulting from magnetic

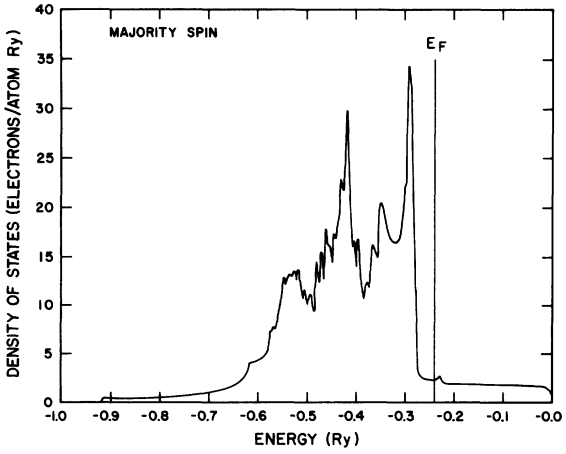

FIG. 3. Projected density of states for minority spin.

FIG. 2. Projected density of states for majority spin.

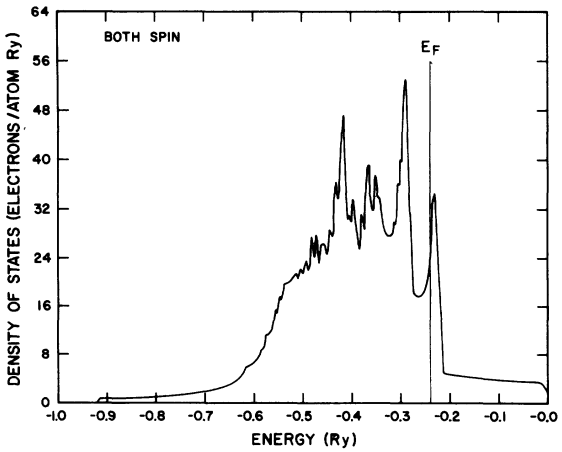

FIG. 4. Total density of states.

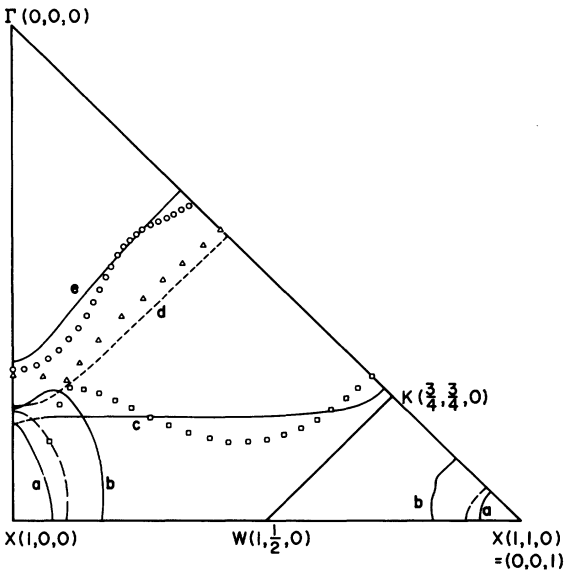

FIG. 5. Fermi-surface cross sections in the (100) plane. The solid and short dashed curves are our results. A solid line indicates that states are predominately (↓) minority spin, the short dashed line indicates majority (↑) spin. The open circles, triangles, and squares are the experimental results of Stark, Ref. 27. The long dashed lines are obtained from an empirical formula given by Tsui (Ref. 26). The sheet (a) is the $X_5\downarrow$ pocket, (b) is the $X_2\downarrow$ pocket, (c) is the Γ centered $d\downarrow$ sheet, (d) is the large ($sp\uparrow$) square, (e) is the small ($sp\downarrow$) square.

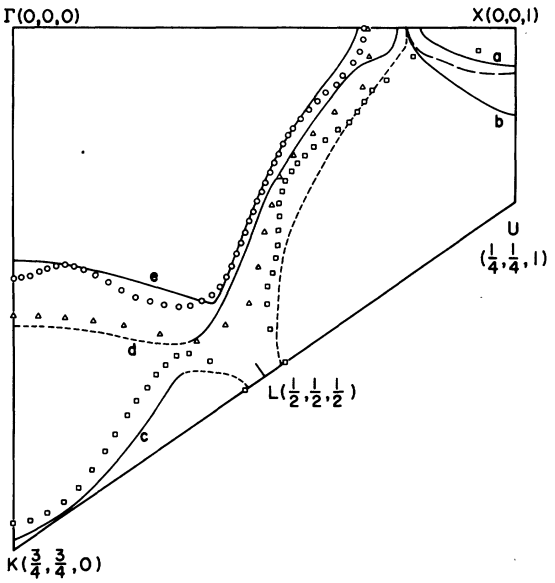

FIG. 6. Fermi surface cross sections in the $(1\bar{1}0)$ plane. The notation is the same as in Fig. 5. Note that the s-$p\uparrow$ neck at L merges in to the large $d\downarrow$ sheet.

breakdown across a small gap resulting from the removal of an accidental degeneracy between spin-orbit split bands.[29]

In our calculation, spins are quantized along the [001] axis. We therefore limited in principle to an investigation of the Fermi surface in the $k_z = 0$ plane. However, the dependence of the band structure on the field direction is probably not large except for the small hole pockets at X, and we will discuss cross sections in a $(1\bar{1}0)$ plane as well. Our Fermi surface cross sections shown in Figs. 5 and 6, where they are compared with recent results of Stark[27] for the large portions of the surface and of Tsui[26] concerning the hole pocket at X. Stark has derived Fermi surface radii from his measurements using the kubic harmonic expansion method of Mueller and Priestly.[30] His inversion program included seven kubic harmonics. We have plotted the Fermi surface radii obtained in this manner on the figures. An empirical formula given by Tsui has been used to outline an experimentally determined cross section for the small hole pocket at X. Some numerical results for dimensions of the $X_5\downarrow$ hole pocket are given in Table II and extremal areas are listed in Table III. Comparisons are made with experiment[25-27] and with the calculations of Zornberg.[10]

There is a substantial degree of agreement between the theoretical and experimental results. It is apparent that the band calculation is able to describe the major pieces of Fermi surface correctly. The most significant disagreement concerns the $X_{2\downarrow}$ hole pocket, which is not observed experimentally, but is predicted by our calculations. Since this pocket is predicted by other band calculations using a local-exchange potential,[16] it is possible that this prediction indicates a basic inadequacy of the local-exchange approximation.

TABLE II. Comparison of $X_5\downarrow$ hole pocket dimensions in atomic units. Numbers underlined are dimensions in the plane normal to the applied magnetic field. These dimensions contribute to the observed dHvA areas.

	Location of pocket	$k_{X\Gamma}$	k_{XW}	k_{XU}
Present calc.	(0, 0, ±1)	0.179	<u>0.077</u>	<u>0.076</u>
	(±1, 0, 0)	<u>0.195</u>	$W(1, 0, \frac{1}{2})$ 0.080	0.076
			$W(1, \frac{1}{2}, 0)$ <u>0.077</u>	
Ref. 10	(0, 0, ±1)	0.201	<u>0.092</u>	<u>0.095</u>
(Parameter set IV)	(±1, 0, 0)	<u>0.218</u>	$W(1, 0, \frac{1}{2})$ 0.096	0.104
			$W(1, \frac{1}{2}, 0)$ <u>0.104</u>	
Ref. 25	(0, 0, ±1)	0.184	<u>0.095</u>	<u>0.089</u>
	(±1, 0, 0)	<u>0.208</u>	<u>0.106</u>	0.102
Ref. 26		0.207	0.099	0.087

TABLE III. Extremal areas of Fermi-surface cross sections in atomic units. Refer to Figs. 5 and 6 for designations.

Band	Present results	Ref. 10	Ref. 25	Ref. 26	Ref. 27
Small square ($sp\downarrow$)	0.84	0.86	1.12		0.90
Large square ($sp\uparrow$)	1.24	1.18	1.33		1.15
Γ centered $d\downarrow$ sheet	2.20	2.05	2.25		
X_5 ($d\downarrow$) pocket (1, 0, 0)	0.038	0.0665		0.0665	
(0, 0, 1)	0.018	0.0270		0.0270	
X_2 ($d\downarrow$) pocket (1, 0, 0)	0.144			Not observed	
(0, 0, 1)	0.089				

Goy and Grimes have observed cyclotron resonance associated with the majority spin Fermi surface neck at L, the hole pocket $X_{5\downarrow}$ and, according to our interpretation, the two large pieces of Fermi surface around Γ. The wave functions associated with the smaller piece have predominately $e_{g\downarrow}$ symmetry near the Γ-X line, but mix components of s-$p\downarrow$ and $t_{2g\downarrow}$ near Γ-K. The states associated with the larger, nearly square section, are of predominately majority spin but have the same spatial symmetry as those on the smaller square, except near the [100] axis where there is a strong, spin-orbit-induced mixing with minority spin d band states.

The experimentally observed cyclotron effective mass has been compared with the effective mass m_c^* obtained from the band structure according to the formula

$$\frac{m_c^*}{m}=\frac{\hbar^2}{\pi}\left(\frac{dA}{dE}\right)_{E_F}, \tag{4.1}$$

in which m is the free-electron mass, and A is the area of the cyclotron orbit. Our results and the experimental findings are presented in Table IV. The results of the semiempirical calculation of Zornberg[10] are also shown. It will be seen that the agreement is fairly good for the $X_{5\downarrow}$ pocket, with the deviation between theory and experiment being of the amount and direction expected to allow for a reasonable enhancement through the electron-phonon interaction. However, our result for the minority spin square is larger than the experimental value, while that for the majority spin square is much smaller than that observed.

TABLE IV. Effective mass associated with Fermi-surface portions. Refer to Figs. 5 and 6 for designations.

Band	Ref. 28	Present results	Ref. 10 parameter set IV
Γ centered $d\downarrow$ sheet		8.84	8.0
Large square ($sp\uparrow$)	5.09	2.22	2.9
Small square ($sp\downarrow$)	4.33	4.75	3.7
X_5 pocket ($d\downarrow$)	0.75	0.66	0.89
X_2 pocket ($d\downarrow$)	Not observed	1.97	

V. OPTICAL CONDUCTIVITY

We have calculated the interband optical conductivity of nickel. We will present results in two cases: (i) including a phenomenological constant relaxation time τ, and (ii) in the limit $\tau\to\infty$ so that the band states are sharp. The general expression for the conductivity tensor in case (i) is obtained from the Kubo formula[31]

$$\sigma_{\alpha\beta}(\omega)=\frac{iNe^2}{(\omega+i/\tau)}\left(\frac{1}{m^*}\right)_{\alpha\beta}-\frac{2ie^2}{m^2\hbar}\times\sum_{\substack{l\vec{k}\\ o}}\sum_{\substack{n\vec{k}\\ u}}\left(\frac{(\omega+i/\tau)}{\omega_{nl}}\mathrm{Re}(\pi_{ln}^{\alpha}\pi_{nl}^{\beta})+i\,\mathrm{Im}(\pi_{ln}^{\alpha}\pi_{nl}^{\beta})\right)\frac{1}{\omega_{nl}^2-(\omega+i/\tau)^2}\,. \tag{5.1}$$

The quantities π_{ln}^{α}, etc., are the Cartesian components of the matrix element vector defined by Eq. (3.2); N is the electron density, τ is the relaxation time, here assumed to be a single constant, ω_{nl} is the energy difference between bands n and l,

$$\omega_{nl}=\hbar^{-1}[E_n(\vec{k})-E_l(\vec{k})], \tag{5.2}$$

and m^* is the optical effective mass. The sum over $n\vec{k}$ includes unoccupied states only while that over $l\vec{k}$ includes occupied states only. The optical effective mass is specified by

$$\left(\frac{N}{m^*}\right)_{\alpha\beta}=\sum_{\substack{l\vec{k}\\ o}}\left(\frac{1}{m_l^*(\vec{k})}\right)_{\alpha\beta}, \tag{5.3}$$

where

$$\left(\frac{m}{m_l^*(\vec{k})}\right)_{\alpha\beta}=\delta_{\alpha\beta}+\frac{2}{\hbar m}\sum_n\mathrm{Re}\frac{\pi_{ln}^{\alpha}\pi_{nl}^{\beta}}{\omega_{nl}} \tag{5.4}$$

and the sum in (5.4) includes all $n\neq l$.

The ordinary optical properties of ferromagnetic nickel are determined by the diagonal components of σ (we have $\sigma_{xx}=\sigma_{yy}\neq\sigma_{zz}$, z being the direction of spin alignment). The result of setting $\alpha=\beta$ in (5.1) is

$$\sigma_{\alpha\alpha}(\omega)=\frac{iNe^2}{(\omega+i/\tau)}\left(\frac{1}{m^*}\right)_{\alpha\alpha}-\frac{2ie^2}{m^2\hbar}(\omega+i/\tau)\times\sum_{\substack{l\vec{k}\\ o}}\sum_{\substack{n\vec{k}\\ u}}\frac{|\pi_{ln}^{\alpha}|^2}{\omega_{nl}}\,\frac{1}{\omega_{nl}^2-(\omega+i/\tau)^2}\,. \tag{5.5a}$$

It can be directly verified that this expression satisfies the sum rule

$$\int_0^{\infty}\mathrm{Re}(\sigma_{\alpha\alpha})d\omega=\pi Ne^2/2m\,, \tag{5.6}$$

where m is the free electron mass. In the limit in which the band states are sharp ($\tau \to \infty$), we obtain the familiar expression for the real part of the conductivity for positive frequencies

$$\mathrm{Re}[\sigma_{\alpha\alpha}(\omega)] = \frac{\pi N e^2}{2(m^*)_{\alpha\alpha}}\,\delta(\omega) + \frac{\pi e^2}{m^2\hbar\omega} \times \sum_{\substack{lk \\ o}} \sum_{\substack{nk \\ u}} |\pi^{\alpha}_{ln}|^2 \delta(\omega - \omega_{nl}) . \tag{5.5b}$$

The off-diagonal components of the conductivity vanish except for σ_{xy} (and σ_{yx}). In this case, we have

$$\sigma_{xy} = \frac{2e^2}{m^2\hbar} \sum_{\substack{lk \\ o}} \sum_{\substack{nk \\ u}} \frac{\mathrm{Im}(\pi^x_{ln}\pi^y_{nl})}{\omega^2_{nl} - (\omega + i/\tau)^2} . \tag{5.7a}$$

The sharp limit of this formula is, for positive frequencies,

$$\mathrm{Im}[\sigma_{xy}(\omega)] = \frac{\pi e^2}{m^2\hbar\omega} \sum_{\substack{lk \\ o}} \sum_{\substack{nk \\ u}} \mathrm{Im}(\pi^x_{ln}\pi^y_{nl})\delta(\omega - \omega_{nl}) . \tag{5.7b}$$

If the matrix elements in these expressions are treated as constants, the conductivity is proportional to the joint density of states. We have computed this quantity by the same method described in Sec. III in connection with the ordinary density of states. The joint density of states is dominated by an enormous spike, resulting from the nearly parallel upper d bands, especially in the region X-W-L. However, the approximation in which the matrix elements are treated as constant is a bad one since in particular the transition associated with this spike has a very weak matrix element. (The states involved in the spike are predominately of opposite spin, and the matrix element would vanish except for the mixing of opposite spin components in the wave function.)

We have calculated the optical conductivity including the $\vec{k}$ dependence of all matrix elements both in the sharp limit, Eqs. (5.5b) and (5.7b), and with the inclusion of a relaxation time. The integration was performed by the method described in Sec. III, in which the $\vec{k}\cdot\vec{p}$ method was used to calculate the energy for $\vec{k}$ corresponding to a subdivided mesh in the Brillouin zone. The momentum matrix elements at the additional mesh points were found by linear interpolation between the values calculated at the basic 1357-point grid. Numerical tests showed that the contribution of the spin-orbit coupling term to the matrix element $\vec{\pi}_{nl}$ [Eq. (3.2)] was negligible for the determination of both the diagonal and off-diagonal elements of the conductivity. We therefore replaced $\vec{\pi}_{nl}$ by $\vec{p}_{nl}$ throughout the calculation. This implies that the off-diagonal conductivity should be regarded as being produced by the modification of the band wave functions produced by the spin-orbit interaction.

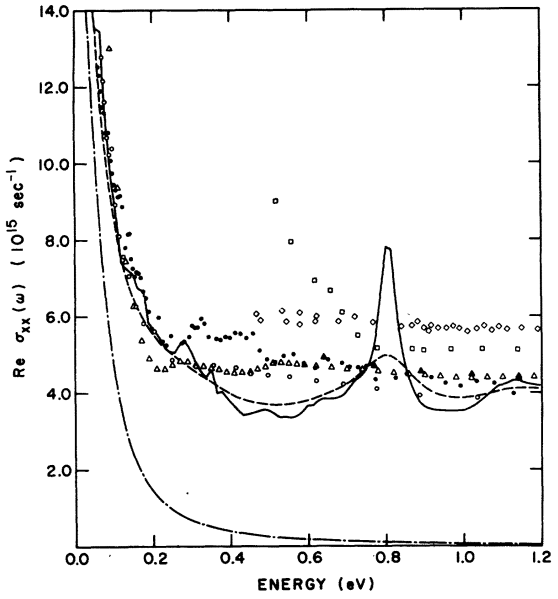

FIG. 7. Real part of the xx component of the conductivity tensor from 0 to 1.2 eV. Long dashes indicate the empirical Drude term [Eq. (5.8)]; solid curve, the interband contribution in "sharp" limit, plus the Drude contribution, dashed curve, the interband contribution with ($\hbar/\gamma = 0.06$ eV) plus the Drude contribution. Experimental results are shown as follows: □, Ref. 33; ◇, Ref. 35; △, Ref. 34; ▲, Ref. 38, ○, Ref. 37, ●, Ref. 36.

Our results for the real part of σ_{xx} between 0 and 1.2 eV are shown in Fig. 7. The solid line represents the contribution from the interband conductivity in the sharp limit ($\tau \to \infty$) to which has been added an empirical Drude term

$$\sigma_D(\omega) = \frac{\sigma_0}{1 + \omega^2\tau^2} , \tag{5.8}$$

in which the constants have been taken to be $\sigma_0 = 18.6\times10^{15}$ sec^{-1} and $\tau = 11.3\times10^{-15}$ sec as determined by Lenham and Treherne.[32] The dashed curve is the sum of the same empirical Drude term plus an interband contribution computed assuming a relaxation time $\hbar/\tau = 0.06$ eV. We have also computed $\mathrm{Re}(\sigma_{zz})$, which is not the same as $\mathrm{Re}(\sigma_{xx})$ in the present case. However, the differences are quite small and are not significant on the scale of this graph. The conductivity in the energy region 1.0–6.0 eV is shown in Fig. 8. The experimental results of several authors[33-38] are also shown in these figures. Although there is a large amount of scatter in the experimental data, there is a reasonable degree of general agreement between many of the measurements, particularly

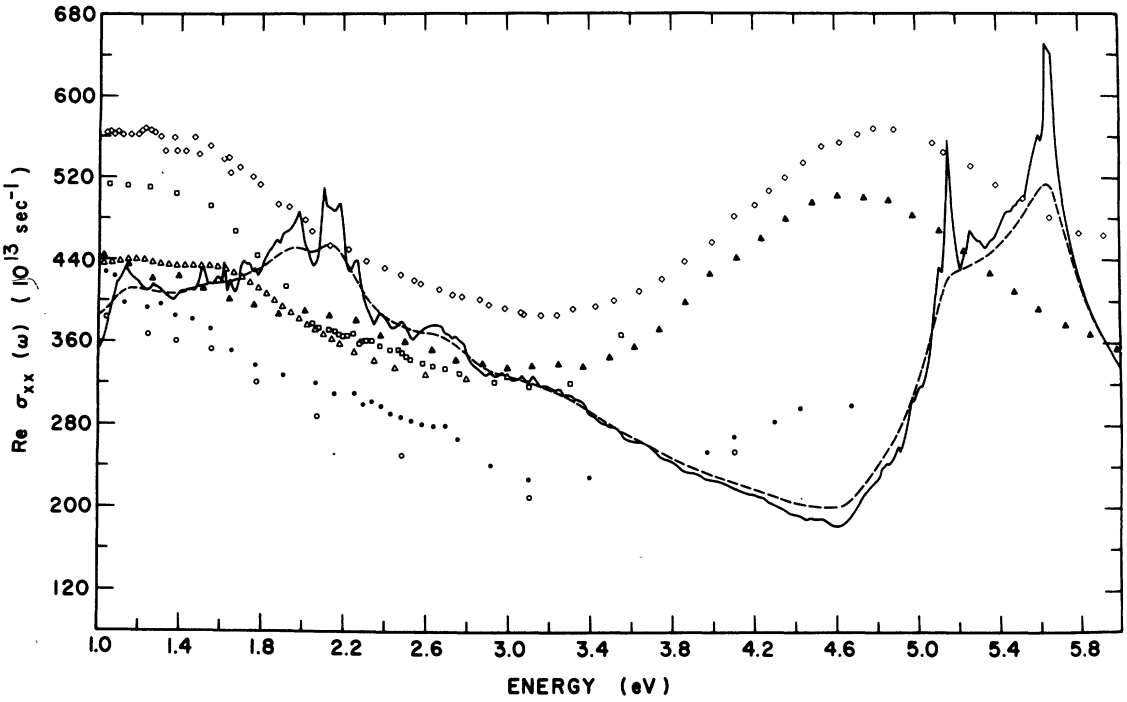

FIG. 8. Real part of σ_{xx} from 1.0 to 6.0 eV. Notation is the same as in Fig. 7.

in regard to the magnitude and the general trend. There is less agreement in regard to detailed structure. We believe that it is significant that our calculations are in good agreement with the general magnitude of the observed conductivity in the low-energy region. In particular, the departure from the Drude term seems to be given satisfactorily. There is little agreement between theory and experiment in regard to specific structures at low energies except, possibly in the 0.2–0.5-eV region where structure in our calculated conductivity appears in some of the observations and is confirmed by thermoreflectance measurements.[39]

A most important feature of our calculated results is the peak at 0.80 eV which results from transitions between the nearly parallel upper d bands near the zone face. This transition is a direct measure of the exchange splitting responsible for ferromagnetism. This peak is quite pronounced when the band states are considered to be sharp; however, it is much reduced if reasonable allowance is made for finite lifetimes of the states. We do not notice any comparable structure in the experimental data in this energy region, and we infer from this discrepancy that our calculation has probably overestimated the exchange splitting. It is not obvious from the data available to us whether or not this transition has actually been observed; however, we tentatively suggest that the broad rise beginning at 0.5 eV in the results of Lynch *et al.*[34] may be associated with this transition. If this interpretation is correct, the d band exchange splitting is about 0.5 eV, in fair agreement with other estimates,[10] and significantly smaller than our calculated value.

Some structure is present in our calculated conductivity in the 2–3-eV range, but this is much reduced when lifetime broadening is included. Failure to observe structure in this energy range[40] suggests that lifetime effects are indeed appreciable. At higher energies, the experimental conductivity shows a large increase, beginning near 4 eV. A corresponding feature is present in our results, but it is displaced to higher energies by about 1 eV. In our calculations, this peak results from transitions between the lower s-d bands and the s-p bands above the Fermi energy. The bands involved are in the outer part of the Brillouin zone, along the Σ axis, and in the vicinity of the symmetry points X and L. The discrepancy in energy between theory and experiment is probably an indication of the inadequacy of our use of atomic wave functions rather than separated orbitals to represent s- and p-like states.

The absorptive part of the off-diagonal elements of the conductivity tensor can be determined from measurements of the ferromagnetic Kerr effect.[41] This effect involves spin-orbit coupling in an essential way. Previous calculations have been

based on perturbation theory and simple models of the band structure.[42] A major conflict developed between the results of different measurements.[43,44] However, more recent work[45-49] has tended to confirm, in a general way, the results of Krinchik and collaborators.

We have calculated the off-diagonal element σ_{xy} of the conductivity tensor. Our results for $\omega\,\mathrm{Im}(\sigma_{xy})$ are shown in Fig. 9, where they are compared with results of Yoshino and Tanaka,[45] Krinchik and Artemjev[47] and Erskine and Stern.[49] Our calculated results do not include any intraband contribution[50] since the experimental data do not extend to low enough energies to permit determination of this quantity. Such a term would simply shift the calculated curves by a constant. The theoretical curves have the same general shape and order of magnitude as the experimental ones. However, the agreement in detail is not particularly good. The negative portion of ϵ_{xy} at low energy can be interpreted as indicating the dominance of transitions of minority spin electrons.[49] The experimental curves become positive at a lower energy than the theoretical results. This is presumably a consequence of our overestimation of the exchange splitting. The negative peak at high energies is found in our calculation to be displaced by about 1 eV with respect to the corresponding experimental feature. A similar result was found for the diagonal elements of the conductivity and the explanation is probably the same. The smooth behavior of the experimental curves probably indicates the presence of substantial lifetime broadening.

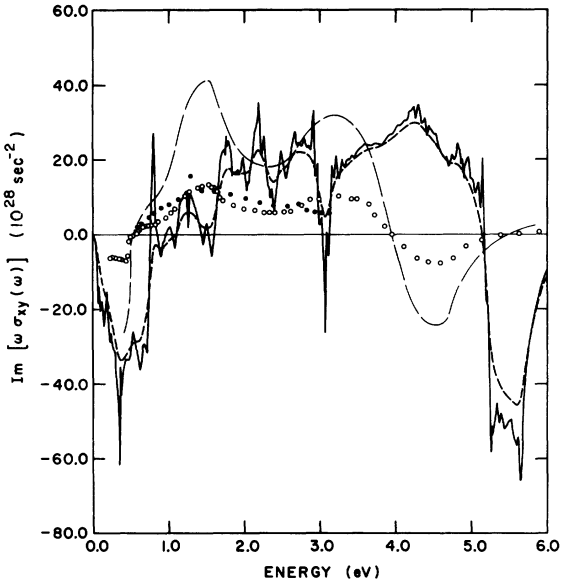

FIG. 9. Imaginary part of σ_{xy} from 0 to 6 eV. The solid curve is the interband conductivity in the "sharp" limit; the short dashed curve is the conductivity calculated with $\hbar/\tau = 0.06$ eV. Experimental results are shown as follows: — — —, Ref. 49, ●, Ref. 45; ○, Ref. 47.

VI. DISCUSSION

We believe that the comparison of the results of this calculation with experiment indicates that simple energy-band theory employing a local exchange potential can successfully predict the essential features of the Fermi surface, and of the optical properties of nickel. Although numerous discrepancies in detail exist, there is a large degree of general agreement between theory and experiment. There is no evidence for unexpectedly large many-body effects, although some of the disagreement between theory and experiment may be due to our use of a simple, single particle approach. This seems particularly likely in regard to the exchange splitting of the upper d bands, which our calculation seems to overestimate. In view of the success of these calculations, and of previous work in which good results are obtained for the charge and magnetic moment distribution,[1] it seems that band theory should provide a basically satisfactory account of the properties of ferromagnetic nickel. The principal obstacles to such a conclusion concern observations of tunneling,[51] and of spin polarized[52-53] photoemission which have been interpreted as indicating a contradiction with the results of band theory. It is possible, however, that detailed calculations of such phenomena based on band theory may remove much of the apparent disagreement.[54,55] We hope to undertake this investigation.

ACKNOWLEDGMENTS

Communications with B. W. Veal and J. H. Weaver are acknowledged. We wish to thank Professor R. W. Stark and Professor P. B. Johnson for giving us unpublished data, and for permission to quote results prior to publication. We have profited from many discussions with Dr. John Kimball.

*Supported in part by the U. S. Air Force Office of Scientific Research.

[1] J. Callaway and C. S. Wang, Phys. Rev. B 7, 1096 (1973).
[2] H. Brooks, Phys. Rev. 58, 909 (1940).
[3] G. C. Fletcher, Proc. Phys. Soc. (Lond.) 67, 505 (1954).

[4]K. Merkle, Z. Naturforsch 14a, 938 (1959).
[5]J. C. Slonczewski, J. Phys. Soc. Jap. 17, S34 (1962).
[6]J. Friedel, P. Lenglart, and G. Leman, J. Phys. Chem. Solids 25, 781 (1964).
[7]L. Hodges, H. Ehrenreich, and N. D. Lang, Phys. Rev. 152, 505 (1966).
[8]G. Allan, G. Leman, and P. Lenglart, J. Phys. (Paris) 29, 885 (1968).
[9]N. Mori, J. Phys. Soc. Jap. 27, 307 (1969).
[10]E. I. Zornberg, Phys. Rev. B 1, 244 (1970).
[11]E. Lafon and C. C. Lin, Phys. Rev. 152, 579 (1966).
[12]A. J. H. Wachters, J. Chem. Phys. 52, 1033 (1970).
[13]J. C. Slater, T. M. Wilson, and J. H. Wood, Phys. Rev. 179, 28 (1969).
[14]W. Kohn and L. J. Sham, Phys. Rev. 140, A1133 (1965); R. Gaspar, Acta. Phys. Hung. 3, 263 (1954).
[15]J. Callaway and J. L. Fry, in *Computational Methods in Band Theory*, edited by P. M. Marcus, J. F. Janak, and A. R. Williams (Plenum, New York, 1972), p. 512.
[16]J. W. D. Connolly, Phys. Rev. 159, 415 (1967).
[17]L. M. Falicov and J. Ruvalds, Phys. Rev. 172, 498 (1968).
[18]The *d-d* portion of the spin-orbit coupling matrix in a cubic crystal, with allowance for cubic symmetry of the crystal potential has been given by J. A. Ricodeau, Phys. Rev. B 7, 4950 (1973).
[19]G. Gilat, J. Comp. Phys. 10, 432 (1972).
[20]G. Gilat and L. J. Raubenheimer, Phys. Rev. 144, 390 (1966).
[21]J. F. Cooke and R. F. Wood, Phys. Rev. B 5, 1276 (1972).
[22]H. Dannan, R. Heer, and A. J. P. Meyer, J. Appl. Phys. 39, 669 (1968).
[23]A. S. Joseph and A. C. Thorsen, Phys. Rev. Lett. 11, 554 (1963).
[24]D. C. Tsui and R. W. Stark, Phys. Rev. Lett. 17, 871 (1966).
[25]L. Hodges, D. R. Stone, and A. V. Gold, Phys. Rev. Lett. 19, 655 (1967).
[26]D. C. Tsui, Phys. Rev. 164, 669 (1967).
[27]R. W. Stark (private communication).
[28]P. Goy and C. C. Grimes, Phys. Rev. B 7, 299 (1973).
[29]J. Ruvalds and L. M. Falicov, Phys. Rev. 172, 508 (1968).
[30]F. M. Mueller, Phys. Rev. 148, 636 (1966); F. M. Mueller and M. G. Priestly, *ibid.* 148, 638 (1966).
[31]R. Kubo, J. Phys. Soc. Jap. 12, 570 (1957).
[32]A. P. Lenham and D. M. Treherne, in *Optical Properties and Electronic Structure of Metals and Alloys*, edited by F. Abeles (North-Holland, Amsterdam, 1966), p. 196.
[33]M. Ph. Stoll, Solid State Commun. 8, 1207 (1970); J. Appl. Phys. 42, 1717 (1971).
[34]D. N. Lynch, R. Rosei, and J. H. Weaver, Solid State Commun. 9, 2195 (1971). We wish to thank Professor Weaver for furnishing corrected values of the conductivity.
[35]M. Shiga and G. P. Pells, J. Phys. C 2, 1847 (1969).
[36]M. M. Kirillova, Zh. Eksp. Teor. Fiz. 61, 336 (1971) [Sov. Phys.—JETP 34, 178 (1972)].
[37]I. I. Sasovskaya and M. M. Naskov, Fiz. Metal Metalloved 32, 723 (1971); 33, 86 (1972).
[38]P. B. Johnson and R. W. Christy (unpublished).
[39]J. Hanus, J. Feinleib, and W. J. Scouler, Phys. Rev. Lett. 19, 16 (1967).
[40]B. W. Veal and A. P. Paulikas, Intern. J. Magn. 4, 57 (1973).
[41]P. N. Argyres, Phys. Rev. 97, 334 (1955).
[42]B. R. Cooper, Phys. Rev. 139, A1504 (1965).
[43]D. H. Martin, S. Doniach, and K. J. Neal, Phys. Lett. 9, 224 (1964); D. H. Martin, K. J. Neal, and T. J. Dean, Proc. Phys. Soc. (Lond.) 86, 605 (1965).
[44]G. S. Krinchik and G. M. Nurmukhamedov, Zh. Eksp. Teor. Fiz. 48, 34 (1965) [Sov. Phys.-JETP 21, 22 (1965)].
[45]T. Yoshino and S. Tanaka, Optics Commun. 1, 149 (1969).
[46]G. S. Krinchik and V. A. Artemjev, Zh. Eksp. Teor. Fiz. 53, 1901 (1967) [Sov. Phys.-JETP 26, 1080 (1968)].
[47]G. S. Krinchik and V. A. Artemjev, J. Appl. Phys. 39, 1276 (1969).
[48]G. S. Krinchik and V. S. Gushchin, Zh. Eksp. Teor. Fiz. 56, 1833 (1969) [Sov. Phys.-JETP 24, 984 (1969)].
[49]J. L. Erskine and E. A. Stern, Phys. Rev. Lett. 30, 1329 (1973).
[50]J. L. Erskine and E. A. Stern, Phys. Rev. B 8, 1239 (1973).
[51]P. M. Tedrow and R. M. Meservey, Phys. Rev. Lett. 26, 192 (1971).
[52]U. Banninger, G. Busch, M. Campagna, and H. C. Siegman, Phys. Rev. Lett. 25, 585 (1970).
[53]G. Busch, M. Campagna, and H. C. Siegman, Phys. Rev. B 4, 746 (1971).
[54]N. V. Smith and M. M. Traum, Phys. Rev. Lett. 27, 1388 (1971).
[55]B. A. Politzer and P. H. Cutler, Phys. Rev. Lett. 28, 1330 (1972).